Quantum membrane phases in synthetic lattices of cold molecules or Rydberg atoms

Chunhan Feng,[1] Hannah Manetsch,[2] Valery G. Rousseau,[3] Kaden R. A. Hazzard,[4,5] and Richard Scalettar[1]
[1]*Department of Physics and Astronomy, University of California, Davis, California 95616, USA*
[2]*Department of Applied Physics and Materials Science, California Institute of Technology, Pasadena, California 91125, USA*
[3]*Department of Cell Biology and Anatomy, School of Medicine, Louisiana State University Health Sciences Center, New Orleans, Louisiana 70112, USA*
[4]*Department of Physics and Astronomy, Rice University, Houston, Texas 77005, USA*
[5]*Rice Center for Quantum Materials, Rice University, Houston, Texas 77005, USA*

(Received 23 February 2022; accepted 1 June 2022; published 21 June 2022)

We calculate properties of dipolar interacting ultracold molecules or Rydberg atoms in a semisynthetic three-dimensional configuration—one synthetic dimension plus a two-dimensional real-space optical lattice or periodic microtrap array—using the stochastic Green's function quantum Monte Carlo method. Through a calculation of thermodynamic quantities and appropriate correlation functions, along with their finite-size scalings, we show that there is a second-order transition to a low-temperature phase in which two-dimensional "sheets" form in the synthetic dimension of internal rotational or electronic states of the molecules or Rydberg atoms, respectively. Simulations for different values of the interaction V, which acts between atoms or molecules that are adjacent both in real and synthetic space, allow us to compute a phase diagram. We find a finite-temperature transition at sufficiently large V as well as a quantum phase transition—a critical value V_c below which the transition temperature vanishes.

DOI: 10.1103/PhysRevA.105.063320

I. INTRODUCTION

Atomic and molecular platforms for quantum simulation offer the versatility to realize an enormous range of physics, which has recently been extended to physics with extra dimensions by augmenting true spatial extent with internal [1–7] or motional states [8–11] coupled to mimic motion through a lattice in a synthetic dimension. Synthetic dimensions can lend access to many-body Hamiltonians with high levels of control over parameters such as tunneling amplitude and phase in the synthetic dimension, particularly useful for studying gauge fields, disorder, and topological band structures, all of which have been explored in recent experiments, reviewed in Ref. [12].

Recent experiments in ultracold molecules and Rydberg atoms demonstrate their potential as many-body systems with synthetic dimensions. Ultracold molecules' rotational-state-exchanging dipolar interactions have been observed in optical lattices [13–15], they have been trapped in arrays of optical tweezers [16,17], and sophisticated coherent rotational state control of many levels has been demonstrated [18], all the ingredients required to create many-body strongly interacting synthetic dimensions with rotational states of molecules [5,6]. Similarly, rapid advances in optical tweezer arrays of dozens or hundreds of Rydberg atoms [19–23] can be combined with the synthetic dimensions for single Rydberg atoms demonstrated in Ref. [7] to create many-body synthetic dimensions. Ref. [7] specifically used a ladder of alternating s and p Rydberg states, but many alternative level schemes are possible.

Here, we consider an effectively three-dimensional (3D) system constructed from a two-dimensional real-space lattice with one ultracold polar molecule or Rydberg atom per site, extended by a third, synthetic, dimension of molecular rotational states, as illustrated in Fig. 1. We will mostly describe the system for the molecular case, but identical physics will apply for configurations of Rydberg atoms, as discussed below. We show that the system undergoes a quantum phase transition as the dipolar interaction V, which causes angular-momentum exchange between adjacent molecules, is varied relative to the "tunneling" J within the synthetic dimension.

The transition represents the development of a "quantum membrane," or a low-temperature phase in which molecules across the lattice are confined to occupy one of a few spontaneously chosen adjacent sites in the synthetic dimension, a two-dimensional surface fluctuating in the three-dimensional space. Previously, this phase transition was examined using mean-field theories [5], and, in one dimension (1D), with density-matrix renormalization group (DMRG) calculations and analytical solutions in the limit $V/J \to \infty$ [6]. Here, we utilize the stochastic Green's function (SGF) method [24] to perform numerically exact Quantum Monte Carlo (QMC) calculations determining the phase boundary at zero and finite temperature, as well as multiple observables across the phase diagram. We evaluate the average distance between molecules along the synthetic direction, which measures the degree of rotational state confinement into a membrane, as well as thermodynamic quantities such as energy, heat capacity, and entropy, and correlation functions. Varying the lattice size allows a characterization of the phase transition in the thermodynamic limit.

II. MODEL AND METHODOLOGY

Experiments on two-dimensional periodic arrays of ultracold polar molecules in an optical trap or microtrap array with

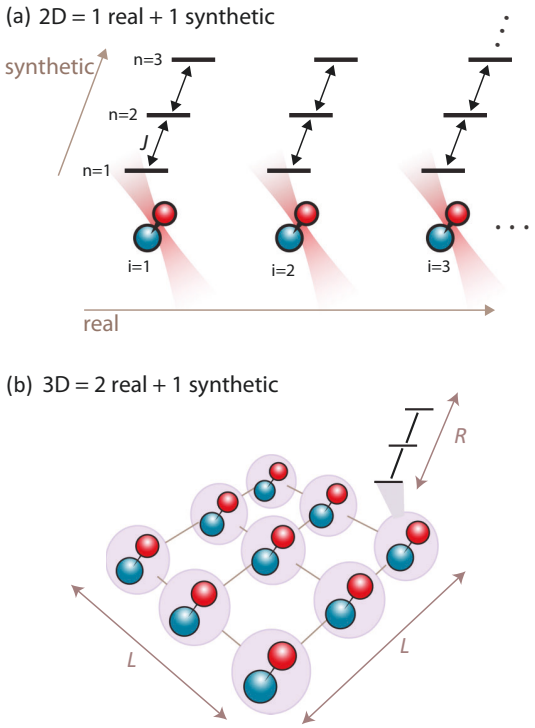

FIG. 1. (a) A one-dimensional (1D) real and 1D synthetic-space lattice of ultracold molecules form an effective two-dimensional (2D) system. Microwaves couple adjacent rotational states with synthetic tunneling rate J. (b) 2D lattices augmented with a synthetic dimension form an effective three-dimensional (3D) system, the focus of this paper.

no real-space tunneling and with near-resonant microwaves coupling a chain of rotational states are described by [5] the many-body Hamiltonian

$$\hat{\mathcal{H}} = -\sum_{i,n} J_n (c^\dagger_{i,n} c_{i,n+1} + c^\dagger_{i,n+1} c_{i,n}) + \sum_{\langle i,j\rangle,n} V_n^{i,j} c^\dagger_{i,n+1} c_{i,n} c^\dagger_{j,n} c_{j,n+1}, \quad (1)$$

when the microwave transition rates, detuning, and interactions are small compared with the energy differences between rotational states. Here $c_{i,n}$ is either a bosonic or fermionic annihilation operator for a molecule at real-space lattice site i and rotational state (synthetic site) n, and the Hamiltonian is the same for both cases, since particles are frozen on their lattice sites and cannot exchange in real space. The first term arises from the near-resonant microwaves, where J_n is proportional to the microwave amplitude coupling states n and $n+1$. The second term arises from dipolar interactions, which drive an exchange of angular momentum n between pairs of molecules with adjacent angular momenta (n_1, n_2), i.e., $(n, n+1) \to (n+1, n)$. We have truncated the $1/r^3$ dipole interaction to nearest neighbors. This captures the dominant interactions, and in 2D the longer range interactions are likely to give mostly quantitative corrections to the physics. More significant qualitative effects are expected only in small regions, for example at low temperatures where multiple phases of matter with nearby energies compete.

Interpreting the rotational states as a *synthetic dimension* indexed by n, the first term describes microwave-induced tunneling along the synthetic dimension for each spatial location i in the array, while the second term describes the dipole interactions, which causes molecules adjacent in the synthetic dimension to undergo coordinated quantum fluctuations. The precise functional forms for $V_n^{i,j}$ are nontrivial [5], but they vary slowly and approach a constant for large n, so we assume $V_n = V$ for all n, an excellent approximation for many choices of rotational states. The J_n are fully tunable in experiment by controlling the microwave amplitudes, but here we restrict to the simplest scenario, in which $J_n = J$ and $V_n^{i,j} = V$. Such a model provides the simplest example of an interacting synthetic dimension in this system, but as has been argued in Refs. [5,6] and we will see here, the physics is already quite rich, with interesting finite-temperature and quantum phase transitions.

In this work, we fix $J = 1$ and $k_B = 1$, while focusing on $V < 0$, where the QMC sign problem is absent [25]. Both signs can be realized in experiment by choosing the polarization of the microwaves. Microwaves that are linearly polarized in the z direction yield a positive sign, while microwaves with a left-circular polarization with respect to the z axis yield the other [5]. We refer to R and L as the linear lattice sizes in synthetic and real space, as illustrated in Fig. 1(b). For a system of trapped ultracold molecules or Rydberg atoms, R is tunable and controlled by the microwave configurations applied. Initial experiments have demonstrated $R = 6$ for Rydberg atoms [7] and demonstrated the individual couplings required for $R = 6$ for molecules [26]. No issues are expected to arise scaling to much larger R, and interesting physics already occurs for $R \leqslant 6$. $N = L \times L$ denotes the total number of real sites (molecules) on a square lattice. We use periodic boundary conditions (PBCs) for both real space and the synthetic dimension. Both open boundary conditions (OBCs) and PBC in synthetic dimensions are realizable experimentally and we do not expect the choice of boundary conditions to alter the physics for large R or L.

The SGF method [24] that we use is closely related to the canonical worm (CW) algorithms [27–30]. It has the advantage of ease of implementation for general forms of interparticle interaction, but is somewhat less efficient than methods which have been optimized for particular models. Its name derives from the central role of the many-body Green's functions and its ability to capture them in a simple and general way. The SGF approach works in the canonical ensemble and utilizes continuous imaginary time. Hence it avoids any systematic errors introduced by Trotter discretization [31–33].

III. RESULTS

A. Thermal phase transition

We begin our determination of the phase diagram by considering a fixed number of rotational states $R = 10$ and $V = -2J$. The temperature dependence of the energy per spatial site E, as obtained by the SGF, is shown in Fig. 2(a) for linear lattice sizes $L = 4, 6, 8, 10$. Figures 2(b) and 2(c)

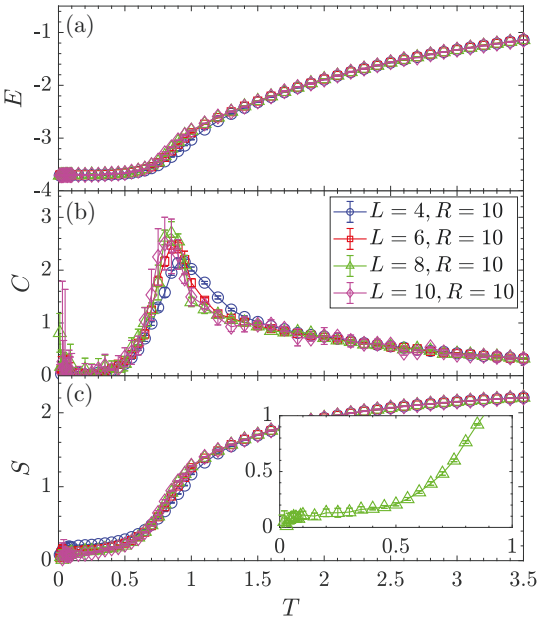

FIG. 2. (a) Energy E, (b) heat capacity C, and (c) entropy S per spatial site as functions of temperature T for $J = 1$ and $V = -2$ for linear lattice sizes $L = 4$, 6, 8, 10 and $R = 10$ synthetic sites. A signature of a phase transition is present at $T \approx 0.8J$. The inset to panel (c) highlights a more subtle feature: an entropy plateau separating the phase transition from a final entropy drop when the temperature is sufficiently small to resolve a nearly degenerate set of states.

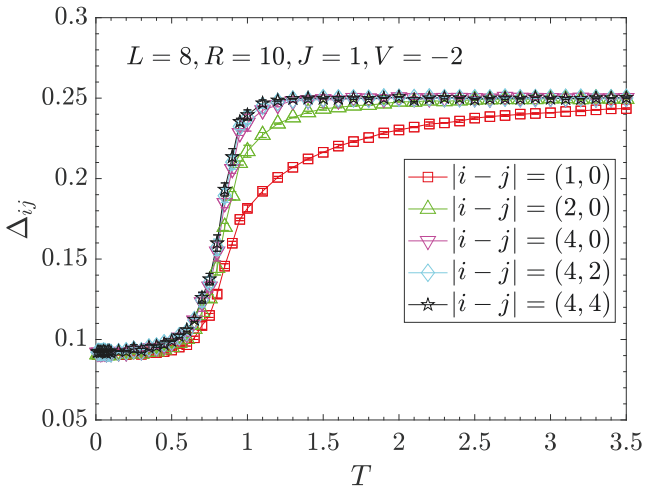

FIG. 3. Average distance Δ_{ij} [Eq. (2)] between the rotational states of molecules on sites i and j, as a function of temperature T, for dimensions $L = 8$, $R = 10$ and energy scales $J = 1$, $V = -2$. A drop, which becomes more abrupt as $|i - j|$ increases, indicates long-range binding of rotational states on different molecules.

complete the picture of the thermodynamics by showing the resulting heat capacity C, and entropy S. $C(T) = dE/dT$ is obtained from a numerical differentiation of the energy. The entropy is obtained by thermodynamic integration, where $T_{\max} \approx 2|V|$ is the highest temperature we simulate. We have checked convergence in $T_{\max}$ and find that it causes only a small shift of the curves and does not change any of the features we identify. We approximate $S(T_{\max}, V)$ by $S(T_{\max}, V = 0)$, the noninteracting entropy at $T_{\max}$, which captures the zeroth-order term in the high-T expansion.

The most prominent feature of Fig. 2 is a sharp decrease in both energy and entropy at $T \approx 0.8J$, and the corresponding peak in $C(T)$. These are signals of a thermal phase transition, as we will verify more rigorously below. In concurrence with this picture, the greater dependence of $E(T)$ on lattice size L in the region $0.7 \lesssim T/J \lesssim 1.2$ suggests a large correlation length.

The inset of Fig. 2(c) focuses on the low-T behavior of the entropy for $L = 8$, $R = 10$, which reveals a plateau in $S(T)$ in a temperature range $0.05J \lesssim T \lesssim 0.3J$ which can be understood as follows: In the limit $J = 0$, the ground state is degenerate [6]. When J is turned on, this ground state degeneracy is broken, so that the resulting unique ground state yields an entropy $S \to 0$ as $T \to 0$. Our value $|J/V| = 1/2$, is sufficiently small that the reduction in entropy occurs in two stages: a phase transition to sheet formation (as we shall show) at $T \approx 0.8J$, and then a final decrease at much lower T when the temperature drops below the energy scale distinguishing the nearly degenerate states, remnants of those exactly present at $J = 0$. There is a corresponding second peak in the heat capacity Fig. 2(b) at $T \approx 0.03J$.

To explore the nature of the ordered phase suggested by the thermodynamics, we measure Δ_{ij}, the average separation in the synthetic dimension between two molecules on spatial sites i and j. This is

$$\Delta_{ij} \equiv \frac{1}{R} \sum_{m,n} |m - n| \langle c^\dagger_{i,m} c_{i,m} c^\dagger_{j,n} c_{j,n} \rangle, \tag{2}$$

where $|m - n|$ denotes the distance between synthetic sites m and n, accounting for periodic boundary conditions.

Measuring Δ_{ij} and related observables discussed below is challenging, but may be possible, in near-term experiments. Experimentally, one can measure populations in specific synthetic sites using standard techniques. In molecules, one can measure populations by state-selective absorption imaging [34] or by absorption imaging the atoms produced after a stimulated Raman adiabatic passage (STIRAP) process addressing specific rotational states [35,36]. However, this can be done only for a single rotational level per experimental shot because the absorption imaging is destructive. Thus one can obtain only the $m = n$ terms in the integrand of Eq. (2). These drawbacks may be overcome by novel imaging techniques, such as dispersive imaging [37] or perhaps by taking advantage of special molecules with quasicycling transitions [38]. In Rydberg atoms, one can measure populations by selective field ionization [39] or level-specific transitions followed by absorption imaging, but novel nondestructive high-resolution real-space imaging will be required to directly measure correlations.

Figure 3 shows Δ_{ij} as a function of temperature for several i, j for an $R = 10$, $L = 8$, $V = -2J$ system. $|i - j|$ denotes the vector connecting real sites i and j. At high temperature, molecules are randomly distributed and densities on different real sites are independent. In this case, defining $P_m(i) \equiv c^\dagger_{i,m} c_{i,m}$, we have $\langle P_m(i) P_n(j) \rangle = \langle P_m(i) \rangle \langle P_n(j) \rangle =$

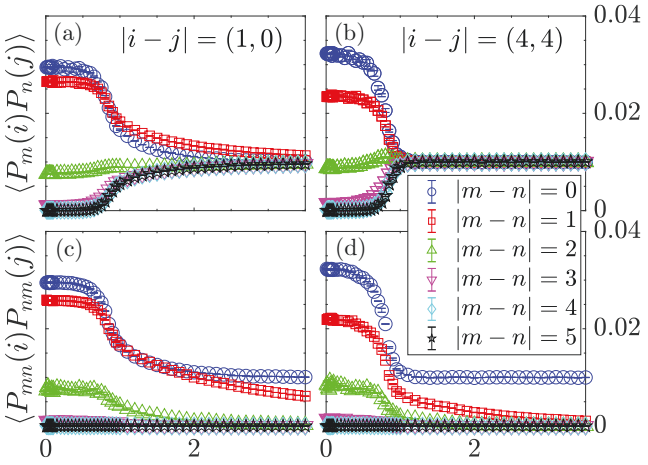

FIG. 4. $\langle P_m(i)P_n(j)\rangle$ and $\langle P_{mn}(i)P_{nm}(j)\rangle$ as functions of temperature T for a $L=8$, $R=10$ system with $J=1$, $V=-2$. As T is reduced below $T\approx 0.8J$ the probabilities that the particles are in nearby synthetic states, $|m-n|=0,1$ rapidly grow, consistent with entry into a membrane phase.

$1/R^2=0.01$ when $i\neq j$. As a consequence, we find $\Delta_{ij}\approx 0.25$ in the high-temperature limit when the sum over m and n is performed, in agreement with the high-T limit of Fig. 3. The transition to the relatively low-value $\Delta_{ij}\approx 0.08$ below $T_c\approx 0.8$J, is consistent with the peak position of $C(T)$ and signals the formation of an ordered quantum membrane phase, with greatly reduced separation in the synthetic dimension.

We can more fully characterize this phase by measuring two additional correlation functions. The first, $\langle P_m(i)P_n(j)\rangle$, breaks the average distance Δ_{ij} into its components and better resolves the rotational separation. When $\langle P_m(i)P_n(j)\rangle$ is measured for the *same* molecule, $i=j$, it takes either of the two temperature independent values $1/R=0.1$ for $n=m$, or $1/R^2=0.01$ for $n\neq m$. On the other hand, for distinct molecules, $i\neq j$, there is a strong temperature dependence. At high T, $\langle P_m(i)P_n(j)\rangle\to 1/R^2$ for all n,m, as discussed above, consistent with a complete lack of correlation between the rotational states. However, as T is lowered, there is a rapid increase in the probability that the rotational states are identical, $|m-n|=0$, or adjacent, $|m-n|=1$. Simultaneously, $\langle P_m(i)P_n(j)\rangle$ becomes small for all $|m-n|>2$. This is true both for neighboring molecules $|i-j|=(1,0)$ and for those at maximal separation $|i-j|=(4,4)$ for $L=8$, indicating the ordering of molecules to nearby synthetic locations is long ranged in real space.

The results of Fig. 3 together with the top row of Fig. 4 give considerable insight into the nature of the phase transition and the ordered phase. At low-temperature, the string is mostly confined to three adjacent states (spontaneously chosen) in the synthetic dimension, and when the system is heated to the phase transition, the width of the strings diverges until it saturates the full width of the synthetic dimension. In an infinite system, it is expected to diverge at the phase transition, as investigated below. Intriguingly, the low-temperature width of the strings is reminiscent of the $J=0$ limit of the 2D = (1 real) + (1 synthetic) system at $T=0$ that was exactly solved in Ref. [6], which had a width of exactly

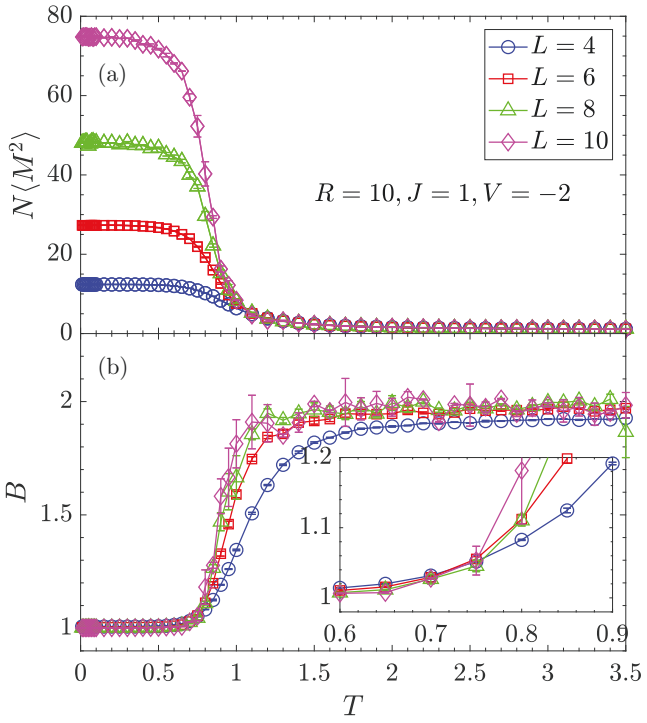

FIG. 5. (a) Structure factor $N\langle M^2\rangle$ as a function of temperature T when $J=1, V=-2$ for $L=4,6,8,10$, $R=10$. (b) Binder ratio $B=\langle M^4\rangle/\langle M^2\rangle^2$ as a function of T. Inset shows a zoom-in showing a crossing at $T_c\approx 0.75$, which coincides with Figs. 2–4.

three synthetic sites. Our results suggest the same phenomena occurs in 3D = (2 real) + (1 synthetic dimension), and that adding J broadens the strings by a finite amount until the phase transition is reached and the string width diverges.

We also consider the correlation function, $\langle P_{mn}(i)P_{nm}(j)\rangle$ with $P_{mn}\equiv c^\dagger_{i,m}c_{i,n}$, which describes the probability of molecules i,j being in states with superpositions of exchanged synthetic positions m,n. As with $\langle P_m(i)P_n(j)\rangle$, the correlation $\langle P_{mn}(i)P_{nm}(j)\rangle$ takes a trivial value $1/R$ for $|i-j|=(0,0)$. For $|i-j|=(1,0)$ and $|m-n|=1$, this rotational exchange is the expectation value of the second (interaction) term of the Hamiltonian (with the coefficient V removed). Figure 4 (bottom) shows this correlation rapidly grows as temperature is lowered below $T\approx 0.8J$. The increase is even more abrupt for larger $|i-j|=(4,4)$. This corroborates the preference for the occupation of nearby rotational states across the entire 8×8 molecular array for $T\lesssim 0.8J$.

We now quantify these transitions through a finite-size scaling analysis and an appropriately defined order parameter. We begin, in analogy to the common analysis of the Potts model [40], by defining an order parameter

$$M\equiv\sum_{m=1}^{R}e^{2\pi im/R}\frac{\sum_j P_j(m)}{N}, \tag{3}$$

which gives a one-dimensional representation of the group of translations in the synthetic dimension. Then $N\langle M^2\rangle$, shown in Fig. 5(a), can be viewed as the corresponding structure factor. Above T_c, the synthetic position is random, and thus

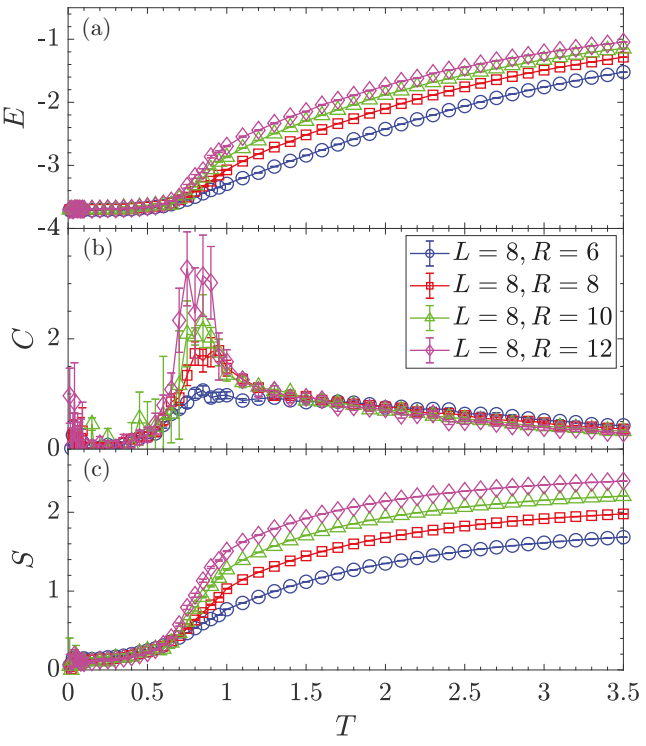

FIG. 6. (a) Energy E, (b) heat capacity C, and (c) entropy S per spatial site as a function of temperature T for $J = 1$, $V = -2$, and $R = 6, 8, 10, 12$.

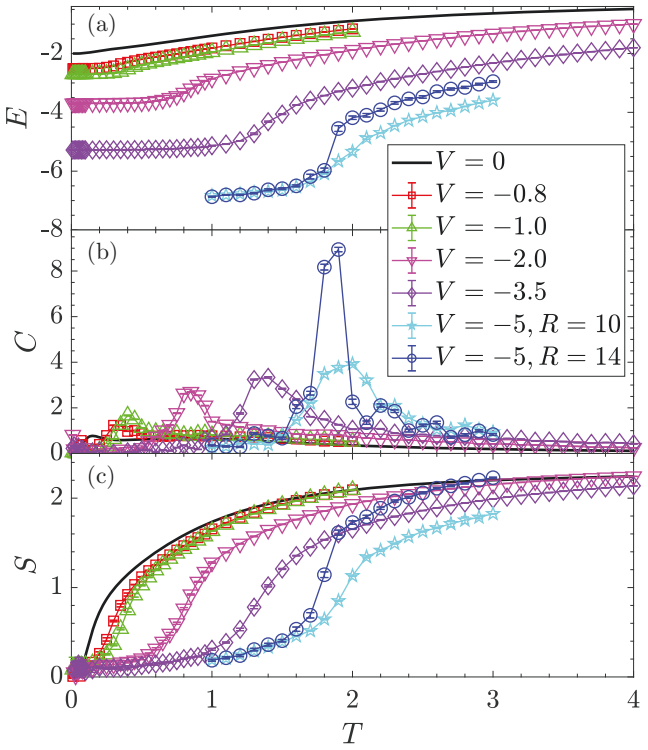

FIG. 7. (a) Energy, (b) heat capacity C, and (c) entropy S per spatial site as functions of temperature T for $J = 1$, $R = 10$, $L = 8$, for interaction strengths $V = -5$, -3.5, -2, -1, -0.8, 0, and for $R = 14$, $V = -5$.

preserves synthetic translation invariance so $\langle M^2\rangle \sim \frac{1}{N} \to 0$ in the thermodynamic limit. Below T_c, in the quantum membrane phase, the structure factor $N\langle M^2\rangle$ becomes proportional to the real-space lattice size N.

An associated Binder ratio [41] is $B = \langle M^4\rangle/\langle M^2\rangle^2$. Its crossings can be used to determine precisely both thermal and quantum critical points. In the molecular gas phase, above T_c, $\langle M^4\rangle \sim 2/N^2$ and the Binder ratio $B \sim 2$. In the quantum membrane phase, below T_c, $\langle M^4\rangle \sim \langle M^2\rangle^2$ and $B \approx 1$. Precisely this behavior is seen in Fig. 5(b). A Binder ratio crossing of curves for different lattice sizes occurs, and is emphasized in the inset. This allows an accurate determination of $T_c = 0.75 \pm 0.02$, refining the more crude T_c estimates from Figs. 2–4.

We now expand our focus from the $R = 10$ results considered so far to study the dependence of the thermal phase transition on R, shown in Fig. 6. When the temperature T is lower than T_c (which can depend on R), molecules collapse to a quantum membrane with thickness of roughly two or three sites and the total energy is independent of the number of unoccupied synthetic sites, as is seen in Fig. 6(a). For $T > T_c$, the energy E depends on R, increasing with R as the molecules escape the bound states. The heat-capacity peaks increase with R, reflecting the greater loss in entropy as the membrane forms and the occupied rotational states decline from $\approx R$ to ≈ 2–3. The positions of the peaks, i.e., the locations of T_c, decrease as R increases, but the shift is relatively small. An analogy is the R-state Potts model, which is a natural generalization of the Ising model (2-state Potts model). The Hamiltonian is given by $H = -J\sum_{\langle i,j\rangle}\delta(s_i, s_j)$, where J is a coupling constant, $\langle i, j\rangle$ denotes the nearest neighbors and each spin s_i has R possible integer states to choose. The critical temperature of the square lattice Potts model, a rough classical analog of the quantum model considered here, is known to decline as $T_c \sim 1/\ln(1+\sqrt{R})$, which similarly has a very slow dependence on R.[1]

We similarly expand our calculations from the previous $V = -2$ to general V. Analogous to Fig. 2, the energy E, heat capacity C, and entropy S are shown in Fig. 7. All the curves are for a 8×8 square lattice with $R = 10$. The black curve is obtained from analytical solution for the noninteracting limit $V = 0$. As V increases, the transition temperature T_c rises and for $|V| \gtrsim 5$, T_c is roughly proportional to V, an expected result since J is negligible and V is the only energy scale at these temperatures. In the noninteracting limit, the ground-state degeneracy is completely removed and entropy drops to $S = 0$ directly without any plateaus. As the interaction strength V grows, wider low-temperature entropy plateaus are evident.

B. Quantum phase transition

The results of Fig. 7 show that T_c is becoming small as V decreases. This suggests the possibility that there is a quantum critical point (QCP) below which there is no ordered phase (no membrane formation) even at zero temperature. To explore

[1]Comparing $R = 6$ and $R = 12$, $1/\ln(1+\sqrt{6}) = 0.808$, and $1/\ln(1+\sqrt{12}) = 0.669$.

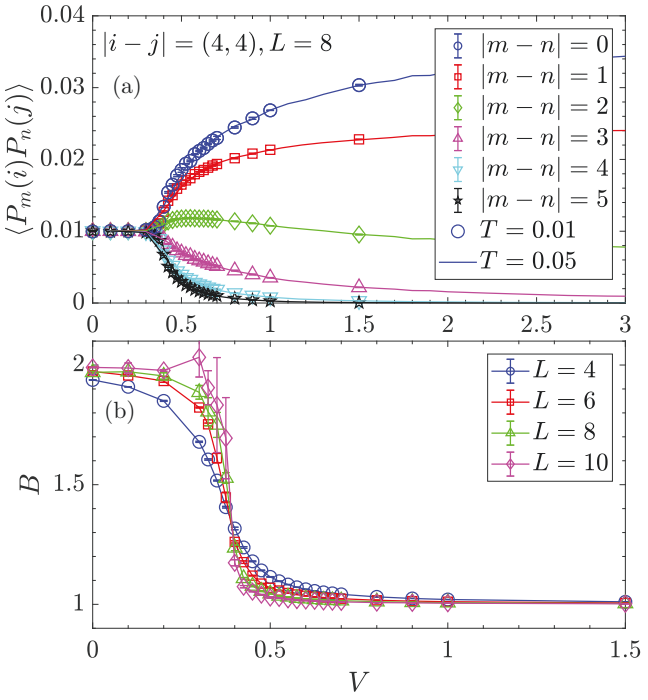

FIG. 8. (a) $\langle P_m(i)P_n(j)\rangle$ as a function of V for a $L = 8$ and $R = 10$ system at low temperatures $T = 0.05,\ 0.01$. (b) The Binder ratio $B = \langle M^4\rangle/\langle M^2\rangle^2$ crossing shows a quantum critical point at $V_c = 0.40 \pm 0.025$.

this possibility, we fix T at a low value and vary the interaction strength V. The correlation function $\langle P_m(i)P_n(j)\rangle$ is plotted in Fig. 8(a). Both $T = 0.05$ (solid line) and $T = 0.01$ (dots) curves are presented. The fact that they coincide indicates we have accessed the ground state for the given finite lattice. The data support the existence of a QCP at $V_c \approx -0.4$. Below this value, even in the ground state, $\langle P_m(i)P_n(j)\rangle = 1/R^2$ for all $|m-n|$, its uncorrelated, gas-phase value. However, for $|V| > 0.4$, the quantum membrane phase occurs at low T. $\langle P_m(i)P_n(j)\rangle$ is then large for $|m-n| \leqslant 2$, whereas $\langle P_m(i)P_n(j)\rangle \approx 0$ for $|m-n| > 2$ away from V_c. The values of $\langle P_m(i)P_n(j)\rangle$ for $|m-n| > 2$ grow as V_c is approached: the membrane becomes increasingly thick.

Similar to the thermal phase transition, a more accurate way to locate V_c is by plotting the Binder ratio B as a function of V for different lattice sizes. The clear crossing of Fig. 8(b) determines the position of the QCP, $V_c = 0.40 \pm 0.025$.

C. Phase diagram

Putting together the results for the thermal and quantum phase transitions leads to the phase diagram shown in Fig. 9. The blue dots are obtained from the peaks in the heat-capacity curves $C(T)$ and the red open circles are extracted from the temperature of largest slope in the average distance $d\Delta_{ij}/dT$. Both data sets were analyzed at fixed spatial lattice size, an 8×8 square with $R = 10$ rotational states. They are in close quantitative agreement. As is suggested in Fig. 6, the dependence of transition temperature T_c on number of rotational states R near this value $R = 10$ is weak.

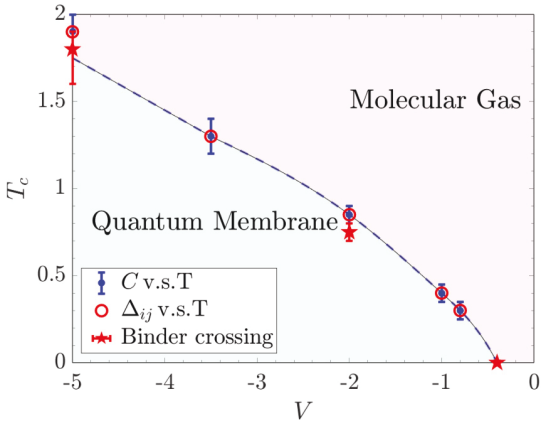

FIG. 9. Phase diagram of the Hamiltonian (1) describing ultracold polar molecules in two spatial dimensions and one synthetic dimension. Transition temperature T_c (obtained from the peak position in heat-capacity curves, the largest slope position in Δ_{ij} versus T plots and the location of the Binder crossing) as a function of V for $R = 10$ system.

As noted earlier, the most reliable T_c are obtained from a Binder crossing, as in Fig. 5 for $V = -2$. These are shown by red stars at $V = -2$ and $V = -5$ in Fig. 9. The Binder value lies somewhat below the values inferred from a single lattice size, an expected result. Finally, the red star at $T_c = 0$ reveals the quantum critical point implied by the Binder crossing in Fig. 8. The two phases are labeled in the figure: When $T > T_c$, the system is in a molecular gas phase where spatially separated molecules are uncorrelated. When $T < T_c$ there is a quantum membrane phase where molecules separated far in real space remain close along the synthetic direction, with $|m-n|$ a finite value, approaching $\lesssim 2$ as $V \to -\infty$.

IV. DISCUSSION AND CONCLUSIONS

In this work we calculated properties of 3D systems formed by two-dimensional (2D) real-space arrays of either ultracold polar molecules or Rydberg atoms augmented by a synthetic dimension employing the stochastic Green's function (SGF) quantum Monte Carlo (QMC) method. Thermodynamic quantities—the energy E, heat capacity C, entropy S—were measured as functions of temperature T and interaction strength V and suggested the occurrence of both finite temperature and quantum phase transitions. The high-temperature 3D gas transitions to a low-temperature quantum membrane, a spontaneously formed fluctuating 2D surface, as evinced by correlation functions that capture the average separation in the synthetic dimension, $[\Delta_{ij}]$, probabilities for two molecules to occupy given synthetic sites $[\langle P_m(i)P_n(j)\rangle]$, and a measure of correlated hopping in the synthetic dimension for particles separated in real space $[\langle P_{mn}(i)P_{nm}(j)\rangle]$. Finite-size studies of these observables, including an analysis of the Binder ratio, suggest a genuine phase transition and capture T_c accurately. Together with the extraction of a quantum critical coupling strength V_c, these data produced a phase diagram in the plane of temperature T and the energy scale V of coordinated quantum tunneling of adjacent molecules.

We show that the quantum membrane phase suggested in prior work [5,6] zero-temperature mean-field or in 2D (1 real + 1 synthetic) DMRG calculations also exists in 3D (2 real + 1 synthetic), and that it survives to finite temperature. We also show this with significantly larger systems and finite-size scaling, and with a variety of conceptually important and experimentally accessible observables. These elucidate the nature of the thermal and phase transitions as a continuous transition occurring by the divergence of the string width. These results will be invaluable for experiments that are beginning to probe synthetic dimensions in arrays of trapped molecules and Rydberg atoms.

A question opened by these results is the precise nature of the classical and quantum phase transitions, in particular their universality class. It is unclear whether this corresponds to a known universality class, or something previously unexplored. Additionally, while the results should capture the main physics, the long-ranged $1/r^3$ interactions will lead to quantitative, and perhaps some qualitative, modifications of the behavior, and will need to be incorporated for detailed comparison with future experiments. Other than practicalities (e.g., molecules have a larger number of stable states, Rydberg atoms have more developed techniques for measuring simultaneous internal state populations), the main difference between cold molecules and Rydberg atoms is potentially the interaction structure. Molecules give the nearly uniform nearest-neighbor interactions in the synthetic direction for natural choices of rotational states. Rydberg atoms naturally give patterned interaction structures if one uses dipole-allowed transitions between states with different principal quantum numbers to realize the synthetic dimension, discussed in Ref. [7]. Interactions are still nearest-neighbor in the synthetic dimension, but alternate in magnitude from bond to bond. In general, both systems have *much* more complicated interaction structures if one either uses alternate choices of rotational or Rydberg states to build the synthetic dimension. Finally, the results and methods also serve as a jumping off point for calculations in the infinite variety of synthetic landscapes that can be experimentally engineered, including topological band structures, such as the Su-Schrieffer-Heeger model realized in Ref. [7], models with disorder, ladders, gauge fields, or even exotic geometries such as Möbius strips. The interplay of the interaction-driven tendency towards a quantum membrane with the single-particle band structures is expected to lead to a rich variety of physics.

ACKNOWLEDGMENTS

The work of C.H.F. and R.T.S. was supported by the grant DOE-DE-SC0014671 funded by the U.S. Department of Energy, Office of Science. We thank Sohail Dasgupta and Bryce Gadway for useful conversations. H.M. was supported by the Research Experience for Undergraduates program (NSF grant PHY-1852581) and by the Caltech Applied Physics Department Yariv/Blauvelt Fellowship. K.H. was supported by the Welch Foundation Grant No. C1872, the National Science Foundation Grant No. PHY1848304, and also benefited from discussions at the KITP, which was supported in part by the National Science Foundation under Grant No. NSF PHY-1748958.

[1] O. Boada, A. Celi, J. I. Latorre, and M. Lewenstein, Quantum Simulation of an Extra Dimension, Phys. Rev. Lett. **108**, 133001 (2012).

[2] A. Celi, P. Massignan, J. Ruseckas, N. Goldman, I. B. Spielman, G. Juzeliūnas, and M. Lewenstein, Synthetic Gauge Fields in Synthetic Dimensions, Phys. Rev. Lett. **112**, 043001 (2014).

[3] M. Mancini, G. Pagano, G. Cappellini, L. Livi, M. Rider, J. Catani, C. Sias, P. Zoller, M. Inguscio, M. Dalmonte, and L. Fallani, Observation of chiral edge states with neutral fermions in synthetic Hall ribbons, Science **349**, 1510 (2015).

[4] M. L. Wall, A. P. Koller, S. Li, X. Zhang, N. R. Cooper, J. Ye, and A. M. Rey, Synthetic Spin-Orbit Coupling in an Optical Lattice Clock, Phys. Rev. Lett. **116**, 035301 (2016).

[5] B. Sundar, B. Gadway, and K. R. A. Hazzard, Synthetic dimensions in ultracold polar molecules, Sci. Rep. **8**, 3422 (2018).

[6] B. Sundar, M. Thibodeau, Z. Wang, B. Gadway, and K. R. A. Hazzard, Strings of ultracold molecules in a synthetic dimension, Phys. Rev. A **99**, 013624 (2019).

[7] S. K. Kanungo, J. D. Whalen, Y. Lu, M. Yuan, S. Dasgupta, F. B. Dunning, K. R. A. Hazzard, and T. C. Killian, Realizing topological edge states with Rydberg-atom synthetic dimensions, Nat. Commun. **13**, 972 (2022).

[8] M. Heimsoth, D. Hochstuhl, C. E. Creffield, L. D. Carr, and F. Sols, Effective Josephson dynamics in resonantly driven Bose–Einstein condensates, New J. Phys. **15**, 103006 (2013).

[9] B. Gadway, Atom-optics approach to studying transport phenomena, Phys. Rev. A **92**, 043606 (2015).

[10] H. M. Price, T. Ozawa, and N. Goldman, Synthetic dimensions for cold atoms from shaking a harmonic trap, Phys. Rev. A **95**, 023607 (2017).

[11] F. A. An, B. Sundar, J. Hou, X.-W. Luo, E. J. Meier, C. Zhang, K. R. A. Hazzard, and B. Gadway, Nonlinear Dynamics in a Synthetic Momentum-State Lattice, Phys. Rev. Lett. **127**, 130401 (2021).

[12] T. Ozawa and H. Price, Topological quantum matter in synthetic dimensions, Nat. Rev. Phys. **1**, 349 (2019).

[13] B. Yan, S. A. Moses, B. Gadway, J. P. Covey, K. R. A. Hazzard, A. M. Rey, D. S. Jin, and J. Ye, Observation of dipolar spin-exchange interactions with lattice-confined polar molecules, Nature (London) **501**, 521 (2013).

[14] K. R. A. Hazzard, B. Gadway, M. Foss-Feig, B. Yan, S. A. Moses, J. P. Covey, N. Y. Yao, M. D. Lukin, J. Ye, D. S. Jin, and A. M. Rey, Many-Body Dynamics of Dipolar Molecules in an Optical Lattice, Phys. Rev. Lett. **113**, 195302 (2014).

[15] F. Seeßelberg, X.-Y. Luo, M. Li, R. Bause, S. Kotochigova, I. Bloch, and C. Gohle, Extending Rotational Coherence of Interacting Polar Molecules in a Spin-Decoupled Magic Trap, Phys. Rev. Lett. **121**, 253401 (2018).

[16] L. Anderegg, L. Cheuk, Y. Bao, S. Burchesky, W. Ketterle, K.-K. Ni, and J. M. Doyle, An optical tweezer array of ultracold molecules, Science **365**, 1156 (2019).

[17] J. T. Zhang, L. R. B. Picard, W. B. Cairncross, K. Wang, Y. Yu, F. Fang, and K.-K. Ni, An optical tweezer array of ground-state polar molecules, Quantum Sci. Technol. **7**, 035006 (2022).

[18] P. Gregory, M. Frye, J. Blackmore, E. Bridge, R. Sawant, J. Hutson, and S. Cornish, Sticky collisions of ultracold RbCs molecules, Nat. Commun. **10**, 3104(2019).

[19] P. Scholl, M. Schuler, H. J. Williams, A. A. Eberharter, D. Barredo, K.-N. Schymik, V. Lienhard, L.-P. Henry, T. C. Lang, T. Lahaye, A. M. Läuchli, and A. Browaeys, Quantum simulation of 2D antiferromagnets with hundreds of Rydberg atoms, Nature (London) **595**, 233 (2021).

[20] D. Bluvstein, A. Omran, H. Levine, A. Keesling, G. Semeghini, S. Ebadi, T. T. Wang, A. A. Michailidis, N. Maskara, W. W. Ho, S. Choi, M. Serbyn, M. Greiner, V. Vuletić, and M. D. Lukin, Controlling quantum many-body dynamics in driven Rydberg atom arrays, Science **371**, 1355 (2021).

[21] S. Ebadi, T. T. Wang, H. Levine, A. Keesling, G. Semeghini, A. Omran, D. Bluvstein, R. Samajdar, H. Pichler, W. W. Ho, S. Choi, S. Sachdev, M. Greiner, V. Vuletić, and M. D. Lukin, Quantum phases of matter on a 256-atom programmable quantum simulator, Nature (London) **595**, 227 (2021).

[22] G. Semeghini, H. Levine, A. Keesling, S. Ebadi, T. T. Wang, D. Bluvstein, R. Verresen, H. Pichler, M. Kalinowski, R. Samajdar, A. Omran, S. Sachdev, A. Vishwanath, M. Greiner, V. Vuletić, and M. D. Lukin, Probing topological spin liquids on a programmable quantum simulator, Science **374**, 1242 (2021).

[23] P. Scholl, H. J. Williams, G. Bornet, F. Wallner, D. Barredo, L. Henriet, A. Signoles, C. Hainaut, T. Franz, S. Geier, A. Tebben, A. Salzinger, G. Zürn, T. Lahaye, , M. Weidemüller, and A. Browaeys, Microwave-engineering of programmable *XXZ* Hamiltonians in arrays of Rydberg atoms, PRX Quantum **3**, 020303 (2022).

[24] V. G. Rousseau, Stochastic Green function algorithm, Phys. Rev. E **77**, 056705 (2008).

[25] E. Y. Loh, J. E. Gubernatis, R. T. Scalettar, S. R. White, D. J. Scalapino, and R. L. Sugar, Sign problem in the numerical simulation of many-electron systems, Phys. Rev. B **41**, 9301 (1990).

[26] J. A. Blackmore, P. D. Gregory, S. L. Bromley, and S. L. Cornish, Coherent manipulation of the internal state of ultracold ^{87}Rb ^{133}Cs molecules with multiple microwave fields, Phys. Chem. Chem. Phys. **22**, 27529 (2020).

[27] H. G. Evertz, G. Lana, and M. Marcu, Cluster Algorithm for Vertex Models, Phys. Rev. Lett. **70**, 875 (1993).

[28] N. Prokof'ev, B. Svistunov, and I. Tupitsyn, Exact, complete, and universal continuous-time worldline Monte Carlo approach to the statistics of discrete quantum systems, J. Exp. Theor. Phys. **87**, 310 (1998).

[29] K. Van Houcke, S. M. A. Rombouts, and L. Pollet, Quantum Monte Carlo simulation in the canonical ensemble at finite temperature, Phys. Rev. E **73**, 056703 (2006).

[30] S. M. A. Rombouts, K. Van Houcke, and L. Pollet, Loop Updates for Quantum Monte Carlo Simulations in the Canonical Ensemble, Phys. Rev. Lett. **96**, 180603 (2006).

[31] H. F. Trotter, Approximation of semi-groups of operators, Pac. J. Math. **8**, 887 (1958).

[32] M. Suzuki, Generalized Trotter's formula and systematic approximants of exponential operators and inner derivations with applications to many-body problems, Commun. Math. Phys. **51**, 183 (1976).

[33] R. Fye, New results on Trotter-like approximations, Phys. Rev. B **33**, 6271 (1986).

[34] D. Wang, B. Neyenhuis, M. H. G. de Miranda, K.-K. Ni, S. Ospelkaus, D. S. Jin, and J. Ye, Direct absorption imaging of ultracold polar molecules, Phys. Rev. A **81**, 061404(R) (2010).

[35] K.-K. Ni, S. Ospelkaus, M. H. G. de Miranda, A. Pe'er, B. Neyenhuis, J. J. Zirbel, S. Kotochigova, P. S. Julienne, D. S. Jin, and J. Ye, A high phase-space-density gas of polar molecules, Science **322**, 231 (2008).

[36] A. Chotia, B. Neyenhuis, S. A. Moses, B. Yan, J. P. Covey, M. Foss-Feig, A. M. Rey, D. S. Jin, and J. Ye, Long-Lived Dipolar Molecules and Feshbach Molecules in a 3D Optical Lattice, Phys. Rev. Lett. **108**, 080405 (2012).

[37] Q. Guan, M. Highman, E. J. Meier, G. R. Williams, V. Scarola, B. DeMarco, S. Kotochigova, and B. Gadway, Nondestructive dispersive imaging of rotationally excited ultracold molecules, Phys. Chem. Chem. Phys. **22**, 20531 (2020).

[38] L. W. Cheuk, L. Anderegg, B. L. Augenbraun, Y. Bao, S. Burchesky, W. Ketterle, and J. M. Doyle, Λ-Enhanced Imaging of Molecules in an Optical Trap, Phys. Rev. Lett. **121**, 083201 (2018).

[39] T. F. Gallagher, *Rydberg Atoms* (Cambridge University Press, Cambridge, 1994).

[40] F. Y. Wu, The Potts model, Rev. Mod. Phys. **54**, 235 (1982).

[41] K. Binder, Finite size scaling analysis of Ising model block distribution functions, Z. Phys. B: Condens. Matter Quanta **43**, 119 (1981).